

SHARPENING THE PRECISION OF THE SUNYAEV-ZEL'DOVICH POWER SPECTRUM

LAURIE D. SHAW,¹ OLIVER ZAHN,² GILBERT P. HOLDER,¹ OLIVIER DORÉ³

Draft version October 31, 2018

ABSTRACT

Using both halo model calculations and a large sample of simulated SZ maps, we demonstrate that high-mass clusters add significant non-Gaussian variance to measurements of the SZ power spectrum amplitude. The difficulty in correctly accounting theoretically for the contribution of these objects to the uncertainty in C_ℓ leads to a reduced sensitivity to σ_8 . We show that a simple solution is to mask out the brightest clusters in the map before measuring the power spectrum. We demonstrate that fairly conservative masking can reduce the variance and Gaussianize the statistics significantly, thus increasing the sensitivity to cosmological parameters. Choosing which objects to mask is non-trivial; we found that using a fixed sky density produced a well-defined and well-behaved estimate that can easily be applied to real maps. For example, masking the 10 (90) brightest clusters in a 100 deg² SZ map will improve the sensitivity to C_ℓ by a factor of two at $\ell = 1000$ (2000) and 1.5 at $\ell = 2000$ (4000). We show that even in the presence of astrophysical foregrounds (primary CMB and point sources) and instrument noise, one can increase the precision on measurements of σ_8 by masking up to 0.9 clusters deg⁻².

Subject headings: galaxies: clusters: general — cosmic microwave background — intergalactic medium
— cosmology:theory — methods: N-body simulations

1. INTRODUCTION

The Sunyaev-Zel'dovich (SZ) effect has long been recognized as a powerful tool for probing the physics of the intra-cluster medium, large-scale structure formation and the dark energy equation of state (Birkinshaw 1999; Carlstrom et al. 2002). Simple but robust analytical arguments (Barbosa et al. 1996; Holder & Carlstrom 2001) and hydrodynamical simulations of clusters (White et al. 2002; Motl et al. 2005; Nagai 2006) have indicated that the integrated SZ flux (the integral of the temperature decrement across the surface area of a cluster) should correlate tightly with cluster mass. Combined with a greater sensitivity than optical or X-ray surveys to high redshift objects, this makes SZ-selected cluster samples well suited for measuring the evolution of the cluster mass function over a wide range in redshift. Experiments such as the Atacama Cosmology Telescope (Kosowsky 2003) and the South Pole Telescope (Ruhl et al. 2004) are currently surveying the microwave sky to develop large catalogs of galaxy clusters that are uniformly selected by the SZ flux.

However, in order to use cluster samples for this purpose, it is necessary to have a good understanding of both the selection function of the survey (Melin et al. 2006; Schäfer & Bartelmann 2007) and of the mapping between the measured integrated SZ flux and cluster mass (and how this evolves with redshift). Besides the slope and normalization of the flux-mass (Y-M) relation, one must also gain some measure of the scatter around the mean relation in order to be able to

differentiate between different dark energy cosmologies (Battye & Weller 2003; Lima & Hu 2005). A detailed characterization of the Y-M relation may require X-ray follow-up of a representative sub-sample of SZ-selected clusters (Majumdar & Mohr 2003). Complete optical coverage of surveyed fields is necessary for obtaining cluster redshifts and to help determine the selection function. Thus, although there is much power in this method, much work is required before it can be applied to its full potential.

The SZ effect can also be detected as a secondary anisotropy in the CMB temperature anisotropy power spectrum, appearing as ‘excess power’ (over the predicted primary anisotropy signal) on angular scales below several arc-minutes. In principle, measuring the SZ angular power spectrum is an easier task than serendipitous cluster detection as one is searching for temperature fluctuations (on a given angular scale) to which clusters over a wide mass and redshift range contribute significantly, without the need to resolve individual clusters at high signal-to-noise.

Predictions for the SZ power spectrum amplitude $C_{\ell, \text{SZ}}$ (henceforth C_ℓ) can be made using the halo model (e.g. Cooray 2001) and estimates of the radial pressure profile of intra-cluster gas. Assuming that the cluster gas resides in hydrostatic equilibrium in the potential well of the host dark matter halo (with an additional steepening of the gas density profile in the outer regions), Komatsu & Seljak (2002) demonstrated that the ensemble averaged power spectrum amplitude \bar{C}_ℓ has an extremely sensitive dependence on σ_8 , where $\bar{C}_\ell \propto \sigma_8^7 (\Omega_b h)^2$. Although there remains a certain ambiguity in the exact amplitude and shape of the predicted signal due to uncertainties in cluster gas physics (and understanding of the contribution of sub-mm and synchrotron sources to the power spectrum provides an added complication), the SZ angular power spectrum represents a

¹ Department of Physics, McGill University, Montreal QC, Canada, H3A 2T8

² Berkeley Center for Cosmological Physics, Department of Physics, University of California, and Lawrence Berkeley National Labs, Berkeley, CA 94720

³ Canadian Institute for Theoretical Astrophysics, 60 St. George, University of Toronto, Toronto, ON, Canada M5S3H8
Electronic address: lds@physics.mcgill.ca

robust observable with which competitive constraints on σ_8 can be obtained.

Rather than attempting to resolve individual clusters, small-scale CMB experiments have focused on detecting SZ power at arc-minute scales and measuring the amplitude of C_ℓ and thus σ_8 . BIMA surveyed 0.2 square degrees on the sky measuring a fluctuation amplitude of $\Delta T^2 = C_\ell \ell(\ell + 1)/2\pi = 220_{-120}^{+140} \mu K^2$, from which they inferred a value of $\sigma_8 = 1.03_{-0.29}^{+0.20}$ (Dawson et al. 2006) and CBI recently measured an excess of 1.6σ above $\sigma_8 = 0.8$ (Sievers et al. 2009). Clearly there is some tension between the value of σ_8 inferred from these experiments and the current value of $\sigma_8 \sim 0.8$ favored by WMAP and X-ray cluster number counts (Dunkley et al. 2009; Vikhlinin et al. 2009). However, we note that recent results from SZA (Sharp et al. 2009) and QUaD (Friedman & QUaD Collaboration 2009) measurements of the SZ power spectrum infer a value of σ_8 that is more consistent with those derived from other methods.

One possible explanation for this discrepancy is that the ICM gas models used to calculate the SZ power spectrum do not include or correctly capture the relevant physics that determine the shape and amplitude of pressure profiles, resulting in a large modeling uncertainty in the amplitude of C_ℓ . Analytic arguments (Holder et al. 2000) and hydrodynamical simulations (da Silva et al. 2001; White et al. 2002) suggest that the inclusion of more detailed physics (radiative cooling, star formation and energy feedback) only moderately influence the amplitude of the power spectrum. This is partly because these effects mostly influence the temperature and density of gas in cluster cores, whereas it is the gas at larger radii that contributes most to C_ℓ (Komatsu & Seljak 2002). However, to date there has not yet been a systematic comparison between simulated and analytic power spectra, partly due to the limited total area of SZ maps that can be produced from the hydrodynamical simulations, and so the actual magnitude of the theoretical uncertainty in C_ℓ remains uncertain.

A second explanation relates to the fact that the probability density function for the field to field distribution of C_ℓ , $P(C_\ell)$, is inherently non-Gaussian, with a long tail towards high values of C_ℓ . The significant non-Gaussian contribution is due to Poisson fluctuations in the sampling of the halo mass function for a given survey field. Hence, although the average power C_ℓ measured over many maps should reproduce the predicted halo model spectrum (assuming the cluster gas physics is correctly modeled), the power measured in any single map may be several times greater than the ensemble-averaged value, if that field happens to contain several very massive clusters. These objects, while not contributing strongly to the mean SZ power spectrum drive the significant non-Gaussian contribution to $P(C_\ell)$. Zhang & Sheth (2007) derived an analytic expression for $P(C_\ell)$ using the halo model approach and demonstrated that the degree of non-Gaussianity is most significant at large angular scales, where massive clusters contribute most of their signal. Until now, it has not been possible to generate a large enough sample of independent simulated SZ maps in order to test the analytic expressions.

The main purpose of this paper is to demonstrate, using both halo model calculations and a large sample of

simulated SZ sky maps generated from a ‘lightcone’ simulation, that the non-Gaussianities in $P(C_\ell)$ are indeed driven by shot noise due to the number of very high mass clusters in a given field, and that one can reduce this Poisson contribution to the total variance in C_ℓ by masking these objects from sky maps. We compare the power spectra measured from our simulated maps with the halo model analytic predictions for C_ℓ and the non-Gaussian contribution to $P(C_\ell)$. In Section 2 we describe the halo approach to calculating the SZ angular power spectrum and trispectrum, and demonstrate how masking clusters will increase the sensitivity of the measured C_ℓ to σ_8 . In Section 3 we compare the analytic and simulated results for C_ℓ , $P(C_\ell)$ and σ_{NG} , and demonstrate in practice the utility of masking the brightest clusters. In Section 4 we discuss the impact of astrophysical foregrounds and instrument noise on our results.

Henceforth, in this paper cluster mass is measured within the spherical region R_{vir} , defined as the region enclosing a mean overdensity of $\Delta_{\text{vir}}\rho_{\text{crit}}$. Δ_{vir} is calculated using the fitting formula provided by Bryan & Norman (1998). The fiducial assumed cosmology has parameters $\Omega_m = 0.27$, $n_s = 0.96$, $\Omega_\Lambda = 0.73$, $\sigma_8 = 0.77$ and $h = 0.72$.

2. SUNYAEV-ZEL'DOVICH ANGULAR POWER SPECTRUM

The thermal SZ effect is a distortion of the CMB caused by inverse Compton scattering of CMB photons (at temperature T_{CMB}) off electrons (at T_e) in the high temperature plasma within galaxy clusters. To first order, the temperature change at frequency ν of the CMB is given by $\Delta T_\nu/T_{\text{CMB}} = f_\nu(x)y$, where $f_\nu(x) = x(\coth(x/2) - 4)$, $x = h\nu/k_B T_{\text{CMB}}$, and y is the normal Compton parameter

$$y = \left(\frac{k_B \sigma_T}{m_e c^2} \right) \int n_e(l) T_e(l) dl, \quad (1)$$

where the integral is along the line of sight. There is a host of higher order effects that can be important at the 10% level, including bulk motions and relativistic effects (Nozawa et al. 2006). Unless stated otherwise we assume henceforth that $f_\nu(x) = -2$, which is appropriate in the Rayleigh-Jeans limit.

We can also calculate the SZ power spectrum, assuming that clusters are Poisson-distributed, by simply summing up the squared Fourier-space SZ profiles, $\tilde{y}(M, z, \ell)$ of all clusters:

$$C_\ell = \int dz \frac{dV}{dz} \int d \ln M \frac{dn(M, z)}{d \ln M} \tilde{y}(M, z, \ell)^2 \quad (2)$$

where $V(z)$ is the comoving volume per steradian and $n(M, z)$ is the number density of objects of mass M at redshift z . For the latter we use the fitting function of Jenkins et al. (2001), while for the SZ profiles as a function of mass and redshift we use either a simple β -model (where $y = y_0(1 + (\theta/\theta_c)^2)^{-1}$) with self-similar scaling for the central y_0 (Holder & Carlstrom 1999) or the hydrostatic model of Komatsu & Seljak (2002) (henceforth referred to as the KS model). We have extensively experimented with different profiles, with most prescriptions showing differences from each other at the level of tens of percent in the power for consistent assumptions about gas fractions and cosmological parameters.

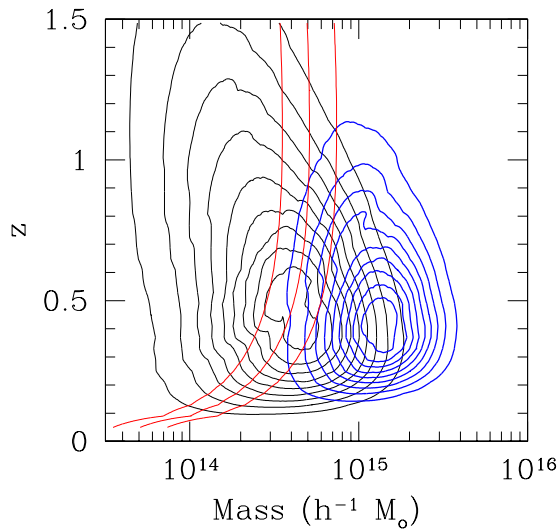


FIG. 1.— Contour plot demonstrating the weight with which clusters of mass M_{vir} at redshift z contribute to the SZ power spectrum (black contours) and trispectrum (blue contours) at $\ell = 2500$. The three lines intersecting the contours are lines of constant integrated SZ flux (Y), each separated by a factor of 2. They demonstrate that one could mask the signal from clusters brighter than some threshold in Y to significantly reduce the trispectrum variance without removing a large fraction of the signal from the power spectrum.

The dominant contribution to the non-Gaussian error comes from the shot noise in galaxy clusters. This Poisson contribution to the variance at a single value of ℓ comes from the one-halo contribution to the trispectrum (Cooray 2001; Komatsu & Seljak 2002; Zhang & Sheth 2007). For closely separated bins in ℓ space, the variance in the SZ power spectrum is given by

$$\sigma^2(C_\ell) = f_{\text{sky}}^{-1} \left[\frac{2C_\ell^2}{(2\ell + 1)\Delta\ell} + \frac{T_{\ell\ell}}{4\pi} \right] \quad (3)$$

where the trispectrum due to shot noise is

$$T_{\ell\ell} = \int dz \frac{dV}{dz} \int d \ln M \frac{dn}{d \ln M} \tilde{y}(M, z, \ell)^4 \quad (4)$$

Henceforth, we will refer to the second term within the brackets in Eqn. 3, as the ‘non-Gaussian’ variance (or trispectrum), σ_{NG}^2 . We will refer to the first term as the ‘Gaussian’ variance, σ_{G}^2 . We note that the ratio of these two quantities is independent of the observed map area f_{sky} .

Figure 1 demonstrates how clusters at a given mass and redshift contribute to C_ℓ and $T_{\ell\ell}$ at $\ell = 2500$ and for $\sigma_8 = 0.77$ (assuming a β -model for the gas pressure profiles). The black and blue contours represent equal contribution to C_ℓ and $T_{\ell\ell}$, respectively. Clusters in the redshift range $0.3 < z < 0.6$ and of mass $4 \times 10^{14} h^{-1} M_\odot$ contribute most to the power spectrum, whereas the trispectrum is driven by clusters at approximately the same redshift but with more than twice the mass. Since the SZ flux scales as $(\text{mass})^{5/3}$, the trispectrum is clearly skewed toward much larger masses than the power spectrum. This leads to a significant amount of non-Gaussianity in the statistics of the SZ power spectrum being driven by the most massive objects.

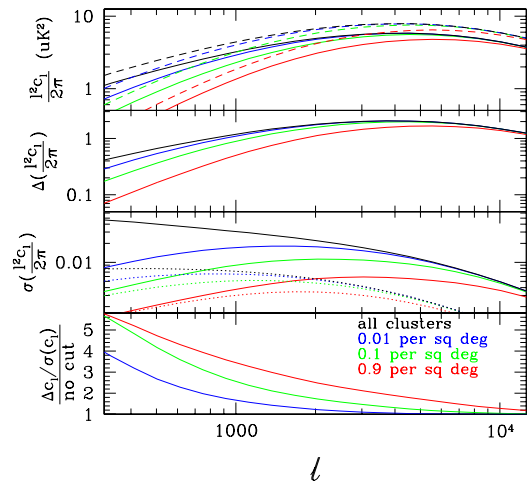


FIG. 2.— (top) The SZ angular power spectrum without masking clusters (black), and masking out the brightest 0.01, 0.1 and 0.9 clusters per square degree (blue, green and red lines). The solid and dashed lines show the results for $\sigma_8 = 0.77$ and 0.80 , respectively. (middle, top) The difference in $\ell(\ell + 1)C_\ell/2\pi$ between the two values of σ_8 for each (un)masked case. (middle, bottom) The standard deviation of the canonical distribution of C_ℓ , as given by Eqn. 3. Note that the value of σ plotted here is calculated assuming full sky coverage ($f_{\text{sky}} = 1$) and for $\sigma_8 = 0.77$. The dotted lines shows the contribution of the purely Gaussian component (σ_{G} , see Eqn. 3). (bottom) The sensitivity of the SZ power spectrum to a change of 0.03 in σ_8 , $\Delta C_\ell/\sigma(C_\ell)$, having masked out clusters divided by the sensitivity for the unmasked case. This panel demonstrates that masking the brightest clusters down to a surface density of 0.9 clusters deg^{-2} improves the sensitivity of the SZ power spectrum to σ_8 by a factor of 3.2 (2.0) at $\ell = 1000$ (4000).

It is clear from Figure 1 that although the most massive clusters do not strongly contribute to the mean power spectrum at $\ell = 2500$, they dominate the trispectrum. These clusters are a significant source of noise in any measurement of C_ℓ . Therefore, if one simply clips the most massive objects from the map, the field-to-field variance of C_ℓ will be reduced and the statistics will become more Gaussian. The three lines intersecting the contours in Figure 1 are lines of constant integrated flux (Y), each separated by a factor of 2. They represent thresholds above which one could mask clusters so that the impact of the trispectrum (or non-Gaussian variance) is greatly suppressed, while not removing a significant amount of signal from a power spectrum measurement. This then allows for a more precise measurement of the ‘true’ or ensemble-averaged SZ power spectrum amplitude, \bar{C}_ℓ , and thus on σ_8 .

Figure 2 demonstrates the improvement in sensitivity to σ_8 when clusters above a given threshold are masked out of the analysis. We define our threshold in terms of a cumulative surface density on the sky, such that all bright clusters down to surface density n_{th} (deg^{-2}) are masked out from the map. We adopt a surface density threshold rather than an integrated flux threshold so that the number of clusters masked is relatively insensitive to σ_8 and modeling of cluster gas physics (see discussion below). In practice we have chosen three values of n_{th} : 0.01 , 0.1 and 0.9 deg^{-2} . SPT has already demonstrated that clusters can be detected at $> 5\sigma$ significance down to the

0.1 deg^{-2} threshold (Staniszewski et al. 2008), and both ACT and SPT are predicted to detect clusters down to the 0.9 deg^{-2} threshold. Therefore, it should be possible for both these experiments to identify and mask or remove clusters down to the thresholds that we examine here.

The top panel in Figure 2 shows the SZ angular power spectrum for no masking (black) and masking down to 0.01, 0.1 and 0.9 clusters per square degree (blue, green and red lines). The solid and dashed lines show the results for $\sigma_8 = 0.77$ and 0.80, respectively. As expected, masking the brightest clusters primarily removes power at larger scales ($\ell < 3000$). Removing the brightest 0.01 clusters per square degree has little impact above $\ell = 1000$, however masking down to 0.1 (0.9) deg^{-2} reduces the power spectrum at this scale by 33% (66%). It is clear that the change in power due to masking is greater than that due to the 0.03 change in σ_8 , so the masking must be included in the theory prediction for the signal.

Although the second panel indicates that an unmasked map has the greatest raw sensitivity to σ_8 , the third panel demonstrates that the masked maps have much lower total variance, and are therefore more precise. The reduced variance more than compensates for the slight reduction in raw sensitivity, such that the ability to use the SZ power spectrum as a cosmological tool is enhanced by using maps with the brightest sources masked. This does not include the extra information encoded in these individually-detected clusters and is based solely on the information in the power spectrum. The bottom panel shows the improvement in true sensitivity ($\Delta(C_\ell)/\sigma(C_\ell)$) having cut out bright clusters, relative to the uncut case. At $\ell = 1000$, masking 0.1 clusters/ deg^2 results in a factor of 2.6 improvement in the cosmological sensitivity of the SZ power spectrum. At $\ell = 3000$ there is still a 50% improvement.

We note that given full knowledge of the number density of clusters and the thermal properties of the ICM over a wide range in mass and redshift, one could construct an optimized scheme for measuring the power spectrum amplitude by de-weighting the signal from high mass clusters. However, as one would already know the cluster mass function – which is more sensitive to cosmological parameters – the power spectrum would then contain no further cosmological information. In the absence of such an optimal estimator, a simple solution is to apply zero weight (i.e. mask) the highest mass clusters from power spectrum measurements (to which they mostly contribute just noise) while utilizing them to sample the cluster mass function, to which they contribute significant statistical information.

We now investigate the difference between applying cuts defined by a surface density or integrated SZ flux threshold. In Figure 3 we plot the fractional error in the amplitude of the SZ power spectrum as a function of angular multipole number (assuming full sky coverage). The black solid and dotted lines show the unmasked results for $\sigma_8 = 0.77$ and 0.87 respectively. The solid blue, green and red curves show the results having applied our normal surface density cuts ($n_{\text{th}} = 0.01, 0.1$ and 0.9 clusters deg^{-2}) for $\sigma_8 = 0.77$. The dotted lines show the fractional error for $\sigma_8 = 0.87$ having applied exactly the

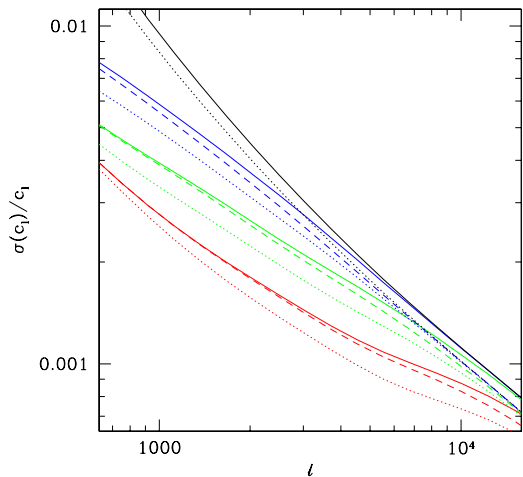


FIG. 3.— The fractional error in the amplitude of the SZ power spectrum as a function of angular multipole number (assuming full sky coverage). Solid lines show the results for $\sigma_8 = 0.77$, having applied no masking (black), and masking the brightest clusters down to a surface density $n_{\text{th}} = 0.01$ (blue), 0.1 (green) and 0.9 (red) clusters deg^{-2} . Dotted lines show the fractional error for $\sigma_8 = 0.87$ having applied the same cut in flux, $Y_{\text{th}}(n = n_{\text{th}})$. Dashed lines show the results for $\sigma_8 = 0.87$ having applied surface density cuts rather than flux cuts.

same cut in flux. The dashed lines show the results for $\sigma_8 = 0.87$ having now used the surface density rather than flux thresholds.

The plot demonstrates that using cuts in surface density produces a fractional error that is approximately independent of σ_8 . On the other hand, adopting a flux threshold means that the number of clusters masked – and thus $\sigma(C_\ell)/C_\ell$ – is highly sensitive to σ_8 . Larger values of σ_8 result in greater numbers of clusters with flux greater than a given value. This will ultimately make the statistical error on measurements of C_ℓ more difficult to determine. Furthermore, the effectiveness of applying flux cuts is also dependent on the accuracy with which one is able to measure cluster fluxes observationally, and the mass and redshift dependence of the intrinsic scatter in the M-Y relation. Using surface density thresholds neatly circumvents these issues.

3. COMPARISONS WITH SIMULATIONS

3.1. Simulations

To date, it has proven difficult to compare the statistics of the SZ power spectrum as predicted by analytic calculations and numerical simulations as the typical box size of hydrodynamical simulations limits the number of independent maps that can be created, while also poorly sampling the extreme high-mass end of the halo mass function. Here we combine an N-body ‘lightcone’ simulation with a semi-analytic model for cluster gas to generate a large number of maps and thus enable such a comparison. We also use our large sample of simulated maps to demonstrate the utility of masking clusters to improve the precision of measurements of the SZ power spectrum.

To generate the simulated SZ maps, we begin with the output of a large ($N = 1260^3 = 2 \times 10^9$ particles) cosmological dark matter simulation. Cosmological param-

eters were chosen to be consistent with those measured from the 3rd-year WMAP data combined with large-scale structure observations (Spergel et al. 2007). The simulated volume is a periodic cube of size $L = 1500h^{-1}\text{Mpc}$; the particle mass $m_p = 1.22 \times 10^{11}h^{-1}M_\odot$ and the cubic spline softening length $\epsilon = 16.5h^{-1}\text{kpc}$. This simulation was carried out with exactly the same methods used for the simulation described in Bode et al. (2007), Sehgal et al. (2007) and Shaw et al. (2008), so for a description of the computational details we refer the reader to these papers.

The very large box size of this simulation makes it ideal for generating a large area of simulated sky. The matter distribution in a light cone extending to $z = 3$ was saved in 348 time slices. Dark matter halos in this light cone were identified with the Friends-of-Friends algorithm using a comoving linking length parameter $b = 0.2$. In total, the lightcone covers a single octant on the sky ($\approx 5000 \text{ deg}^2$), containing over two million clusters with $M_{\text{FOF}} > 10^{13}h^{-1}M_\odot$. For the purposes of the analysis here we retain only clusters with $M_{\text{FOF}} > 3 \times 10^{13}h^{-1}M_\odot$.

The cluster gas distribution in each halo was calculated using the semi-analytic model described in Ostriker et al. (2005) and Bode et al. (2007). In brief, a 3D mesh (with cell side-length $2\epsilon = 33h^{-1} \text{ kpc}$) is placed around each cluster, with the gas pressure and density determined in each mesh cell assuming hydrostatic equilibrium and a polytropic equation of state (with adiabatic index $\Gamma = 1.2$, Ascasibar et al. 2006). It is also assumed that the gas in the densest cluster regions has cooled and condensed, forming stars. At $z = 0$, the stellar/gas mass ratio is set to 0.1 (Lin et al. 2003; Voevodkin & Vikhlinin 2004). To compute the star/gas ratio at $z > 0$, the star formation rate was assumed to follow a delayed exponential model (Eqn. 1 of Nagamine et al. 2006), with decay time $\tau = 1.5 \text{ Gyr}$.

As discussed in detail in Bode et al. (2007), the most important free parameter in this model is the energy input into the cluster gas via non-thermal feedback processes, such as AGN outflows and supernovae. This is set through the parameter ϵ_f , such that the feedback energy is $\epsilon_f M_* c^2$, where M_* is the stellar mass in the cluster. It was demonstrated that setting $\epsilon_f = 3 \times 10^{-5}$ provides good agreement between the $M - T$ and $f_g - T$ scaling relations obtained from our simulation plus gas model cluster sample and those from X-ray observations (Arnaud et al. 2005; Vikhlinin et al. 2006; Gastaldello et al. 2007; O’Hara et al. 2006; Zhang et al. 2007).

From the output of our ICM model, we produce a 2-d ‘postage-stamp’ y image for each cluster by summing up the electron pressure $n_e T_e$ in each mesh cell along one direction (for example, see Fig. 7 of Ostriker et al. 2005). We then construct a library of images for all clusters in the lightcone octant with $M_{\text{vir}} > 2.5 \times 10^{13}M_\odot$. Note that each postage-stamp is produced having rotated the 3D mesh around the cluster so that one face lies parallel to the plane of the lightcone ‘sky’. SZ cluster sky maps are thus produced by projecting down the lightcone, summing up the contribution of all the clusters along the line of sight. In practice, we produce individual SZ sky maps of size 5x5 degrees. We set the image

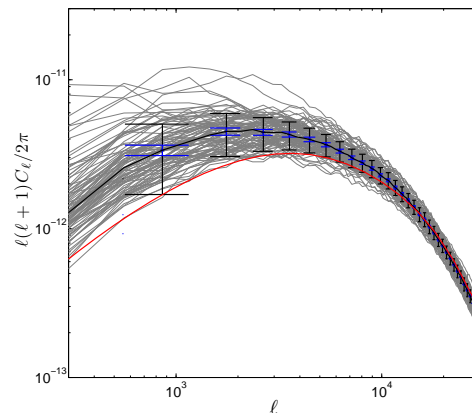


FIG. 4.— SZ angular power spectrum measured for each of the 25 deg^2 simulated maps for our BO sample (grey lines). Black error bars plot the 1σ statistical errors around the mean value \bar{C}_ℓ (black solid line) for the sample. The blue error-bars denote the standard deviation expected from Gaussian cosmic variance alone (the first term in Eqn. 3). The red line denotes the power spectra calculated using the halo model and KS gas profile.

resolution (pixel size) to 0.25 arcminutes. In order to allow robust comparison with the analytic results, we also create a second set of simulated maps in which we replace the gas model cluster ‘postage-stamp’ images with a β -model profile with $\beta = 1$ and normalized in the same way as for the analytic calculation described in the previous Section. We henceforth refer to the maps produced with the Bode et al. (2007) gas prescription as the BO gas model sample. In total we produce 96 25 deg^2 maps (2400 deg^2 in total of simulated sky) for each gas profile.

3.2. Simulated SZ power spectrum and trispectrum

In Figure 4 we plot the SZ angular power spectrum measured for each of the 25 deg^2 simulated maps (grey lines) in our BO gas model sample. The solid black line represents the mean power spectrum measured for the BO gas model maps; the red solid line the halo model predictions for the KS gas model. The black error bars denote the 1σ statistical errors around the mean value \bar{C}_ℓ for the BO map sample. The blue error-bars denote the standard deviation expected from Gaussian cosmic variance alone (σ_G , the first term in Eqn. 3). The simulated power spectra are band-averaged in bins of $\Delta_l = 300$ and are apodized with a 2d Gaussian window function with unity variance. The analytic power spectra have been convolved with a Gaussian of FWHM 0.25 arcminutes in order to approximately account for the pixelisation of the simulated maps. We also note that the analytic power spectra are calculated omitting the contribution of clusters with $M_{\text{vir}} < 2.5 \times 10^{13}M_\odot$. This is because the simulated maps are only 100% complete down to this mass, and so we have omitted lower mass clusters from the simulated sky-maps.

We note that the power spectra measured for the BO gas model simulations agree with the KS power spectra at very small angular scales ($\ell > 10,000$) but have significantly more power at larger scales. This additional power is most likely due to the impact of the feedback parameter in the BO model. The additional energy added to the gas has the effect of heating and ‘puffing out’ the gas, reducing the slope of the pressure profiles in the outer re-

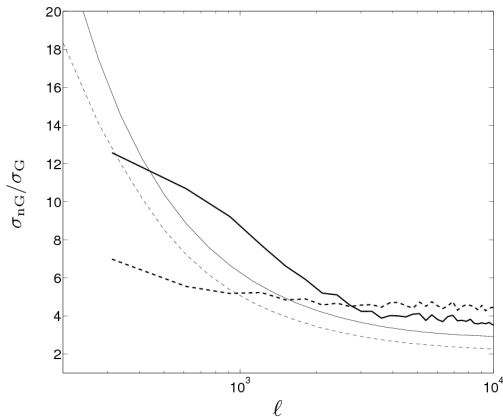


FIG. 5.— Square root of the ratio of the non-Gaussian (trispectrum) to Gaussian contributions to the total variance in C_ℓ , $\sigma_{\text{nG}}/\sigma_{\text{G}}$, as a function of angular multipole number. Heavy solid and dashed lines represent the β -model and BO gas model simulated maps, respectively. Light solid and dashed lines show the results from the halo-model calculation assuming β -model and KS gas profiles.

gions and increasing the large-scale signal. We also note that the KS model has a relatively steep SZ profile at larger radii, reducing the signal at larger scales. The full impact of non-gravitational heating sources on the ICM gas temperature and density profiles is currently poorly understood; the KS prescription is not astrophysically well-motivated and there is no reason to expect the model to match either the BO gas model or real clusters at high redshift. Hence there remains a large theoretical uncertainty in C_ℓ which must be accounted for when attempting to constrain σ_8 via the SZ power spectrum. The exact range of uncertainty in C_ℓ between different models and simulations has not been quantified and we leave this issue to future work. We have confirmed that the power spectra measured from our sample of β -model maps matches the equivalent predictions from the halo model approach.

As demonstrated by the error bars in Figure 4, the total field-to-field variation in the power spectrum amplitude is several times greater than the Gaussian error, with the factor decreasing with increasing ℓ . This is due to Poisson noise associated with the discrete sampling of the halo mass function in each field. Comparing the individual simulated power-spectra to the error-bars, it is also clear that the distribution of C_ℓ is highly non-gaussian, especially for $\ell \leq 6000$. The power spectra for individual maps (grey lines) indicate that the non-gaussian variance is being driven by fields with $C_\ell \gg \bar{C}_\ell$ (where \bar{C}_ℓ represents the mean), corresponding to fields that contain at least one very massive cluster.

In Figure 5 we plot the ratio of the non-Gaussian and Gaussian contributions to the total standard deviation in the statistical distribution of C_ℓ , $\sigma_{\text{nG}}/\sigma_{\text{G}}$ (the second term divided by first term in Eqn. 3), as a function of angular multipole number. The total variance of $P(C_\ell)$ is therefore just the sum of σ_{nG}^2 and σ_{G}^2 , although we reiterate $P(C_\ell)$ is a strongly non-gaussian function at larger scales and thus the total variance (and mean) does not completely define this distribution. σ_{nG}^2 is measured from the simulated maps by calculating the variance in C_ℓ for each set of maps, multiplying this by f_{sky} and

deducting the Gaussian variance, calculated using \bar{C}_ℓ . The heavy lines represent the results for our simulated β -model (solid) and BO gas model (dashed) maps. The thin lines are the equivalent results for the β -model and KS halo model calculations, respectively.

Comparing thick and thin solid black lines, we find that the non-Gaussian error measured for our set of simulated β -model maps is approximately one third greater than that predicted by the trispectrum. As we find a good agreement between the simulated and predicted power spectra, this discrepancy must be due to effects that increase the width of $P(C_\ell)$ without influencing strongly the ensemble-averaged mean. One such effect is the non-linear bias, or small scale halo clustering, which is not accounted for in the trispectrum. As noted in Section 2 and Cooray (2001); Komatsu & Seljak (2002); Zhang & Sheth (2007), the two halo (and higher-order) contribution to the trispectrum – which accounts for the linear bias – is insignificant, including the two-halo term increases σ_{nG} by only a few percent. We have found that by remeasuring σ_{nG} for both sets of simulated maps having first randomised the halo positions reduces $\sigma_{\text{nG}}/\sigma_{\text{G}}$ such that the simulated β -model line becomes into better agreement with that of the trispectrum result, although remains above the predicted curve at all ℓ .

The thick and thin dashed lines in Figure 5 show the ratio of the non-Gaussian to Gaussian variance for BO gas model simulations and the analytic KS model. The simulations demonstrate a shallower dependence on ℓ than the halo model calculation. Given that $\sigma_{\text{G}} \propto C_\ell$, the flatness of the simulated curve is likely due to the larger mean power simulated spectrum in the simulated maps compared to the KS model predictions. We note again however that there is no reason why an agreement is expected. Indeed, as the simulation results include large variations in the underlying dark matter halo structure (including morphology and substructure) we would expect $\sigma_{\text{nG}}/\sigma_{\text{G}}$ to be greater, especially at small angular scales.

3.3. Masking Clusters

In Section 2 we showed that the primary contribution to the SZ power spectrum comes from clusters occupying a different region of the cluster mass-redshift plane to those that determine the trispectrum. Clusters at $z \approx 0.4$ and of mass $4 \times 10^{14} h^{-1} M_\odot$ contribute most strongly to the power spectrum, whereas clusters at $1 - 2 \times 10^{15} h^{-1} M_\odot$ are the foremost contributors to the trispectrum. Therefore, if one wishes to measure accurately the mean SZ power spectrum, very high mass clusters constitute a source of noise. One can mask or remove the brightest clusters detected in a SZ map down to some threshold density in order to suppress the trispectrum contribution to the total variance in C_ℓ without removing a large component of the signal from the power spectrum. We now demonstrate this in practice using our sample of simulated maps.

To evaluate the sensitivity of the SZ power spectrum to σ_8 , we use a second lightcone simulation to create an additional sample of mock SZ maps. The cosmological parameters were chosen to be consistent with those measured from the 5th-year WMAP data (Dunkley et al. 2009), therefore $\sigma_8 = 0.8$ for this simulation (compared to 0.77 as for our WMAP3 run). The simulated volume

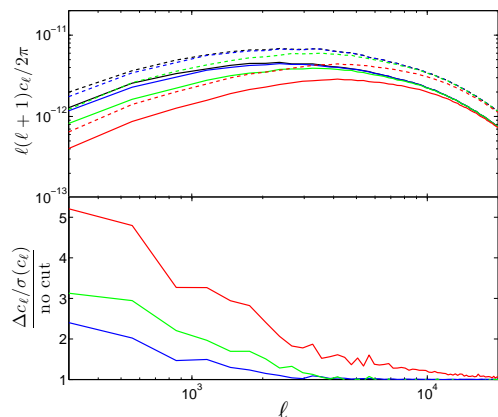


FIG. 6.— (*Upper*) The mean angular power spectrum measured for our WMAP 3 (solid) and 5 (dashed) samples of simulated maps (BO gas model), having applied no masking (black), and masking the brightest clusters down to 0.01, 0.1 and 0.9 clusters deg^{-2} (blue, green and red lines). (*Lower*) The ratio of the sensitivity of the SZ power spectrum to the difference in σ_8 between our two simulations having masked clusters to that with no masking.

is a periodic cube of size $L = 1000h^{-1}\text{Mpc}$; the particle mass $m_p = 6.82 \times 10^{10}h^{-1}M_\odot$ and the cubic spline softening length $\epsilon = 16.28h^{-1}\text{kpc}$. We have applied the Bode et al. (2007) gas prescription to the halos in the WMAP5 lightcone, and created a second set of mock SZ sky maps using the procedure described in the previous section. We refer to the $\sigma_8 = 0.77$ maps as the WMAP3 simulation, and the $\sigma_8 = 0.80$ maps as the WMAP5 simulation.

Clusters are masked from the simulated maps in the following manner. For each of the 96 maps in the WMAP3 & 5 samples, there is an associated catalogue listing all clusters in map. We combine all 96 catalogues and rank-order clusters by their integrated SZ flux Y . Starting with the brightest cluster, we then fit and remove an isothermal β -model (with β fixed at 1) from the map at the location of the cluster. This is then repeated until all clusters down to the desired surface density threshold n_{th} have been masked. This process can be performed in practice on real SZ survey maps by ranking detected clusters by their detection significance, and removing each in turn down to the required threshold surface density (and is somewhat analogous to the application of an optimal matched-filter, Herranz et al. 2002; Melin et al. 2006; Schäfer et al. 2006).

The upper panel of Figure 6 demonstrates the mean power spectrum measured with no clusters masked (black line), and having masked clusters down to 0.01, 0.1 and 0.9 deg^{-2} (blue, green and red lines). The solid lines show the results for our WMAP3 simulation, the dashed lines for our WMAP5 lightcone simulation. For minimal masking, power is removed only on large angular scales, shifting to smaller scales as increasing numbers of clusters are masked. Removing 0.01 clusters per square degree barely changes the average power spectrum, whilst masking 0.1 clusters per square degree reduces power by less than a third at $\ell = 1000$, and negligibly at $\ell > 3000$. Masking 0.9 clusters deg^{-2} removes power over a wide range of scales, reducing the mean band-averaged power by a factor of 2.5 at $\ell = 1000$ and by 27% at $\ell = 5000$. As expected, the most massive clusters contribute most

of their power at large angular scales, and that at scales of $\ell > 5000$ low mass clusters contribute the majority of the signal. These results are similar to those shown in Figure 2.

In the lower panel of Figure 6 we plot the sensitivity of the SZ power spectrum to the difference in σ_8 between the two simulation samples ($\Delta\sigma_8 = 0.03$) including cluster masking, divided by the sensitivity for the unmasked case. We define sensitivity as being the difference in \bar{C}_ℓ between the two simulations divided by the standard deviation in C_ℓ , $\sigma(C_\ell)$ measured in the $\sigma_8 = 0.77$ sample of maps. The line colours are the same as in the upper panel. It is immediately evident that whilst removing down to 0.01 clusters per square degree has little impact on the mean power spectrum, there is a clear gain in sensitivity below $\ell = 1000$. Masking just the 10 brightest clusters per 100 deg^2 improves the sensitivity by a factor of two at $\ell = 1000$ and 1.5 at $\ell = 2000$. Masking the 90 brightest clusters in the same area enables similar improvements at $\ell = 2000$ and 4000. The improvement in sensitivity measured for our simulated maps agrees well with the analytic predictions from the halo model approach (see the lowest panel in Figure 2).

In addition, as one masks out the brightest clusters the PDF of C_ℓ becomes significantly more Gaussian. This is demonstrated in Figure 7, in which we plot the distribution of C_ℓ/\bar{C}_ℓ at $\ell = 1000, 2500, 6000$ and 10,000 for our WMAP3 sample. The unshaded, dashed histogram represents $P(\bar{C}_\ell/\bar{C}_\ell)$ for the unmasked case, the shaded histogram represents $P(C_\ell/\bar{C}_\ell)$ having masked bright clusters down to 0.9 clusters per square degree. For the unmasked case, it is clear that the level of non-Gaussianity is significantly greater at large scales, where massive clusters contribute most of their power. It is also immediately apparent that the masked distribution is significantly more Gaussian than the unmasked case. This can be quantified by the reduction in skewness between the masked and unmasked distributions, which is 1.0, 0.5, 0.2 and 0.1 at $\ell = 1000, 2500, 6000$ and 10,000.

4. IMPACT OF FOREGROUNDS AND NOISE

We have demonstrated the utility of masking clusters from SZ sky maps to reduce the non-Gaussian variance in the amplitude of the SZ power spectrum and thus improve the precision with which one can measure the ensemble-averaged C_ℓ . However, there still remains a question of the overall gain in sensitivity once one accounts for astrophysical foregrounds, such as the primary CMB temperature anisotropies and the contribution from radio and sub-mm point source populations, and instrument noise. While masking bright clusters reduces the field-to-field variance in C_ℓ , the amplitude of the ensemble-averaged C_ℓ is also reduced. Masking increasing numbers of clusters thus reduces the amount of SZ power relative to that of the foregrounds. The variance in the foreground signal is proportional to $C_{\ell,\text{fg}}^2$, therefore as the SZ signal is reduced by masking, the total fractional error on the SZ amplitude due to the error in the foreground signals increases. The relevant question is, how does the total intrinsic error (Gaussian plus non-Gaussian) on the SZ signal $\sigma(C_{\ell,\text{SZ}})$ compare to the error (or uncertainty) on the the primary CMB and point source power spectra amplitudes within a given field?

If σ_{NG} dominates the error in the total power measured

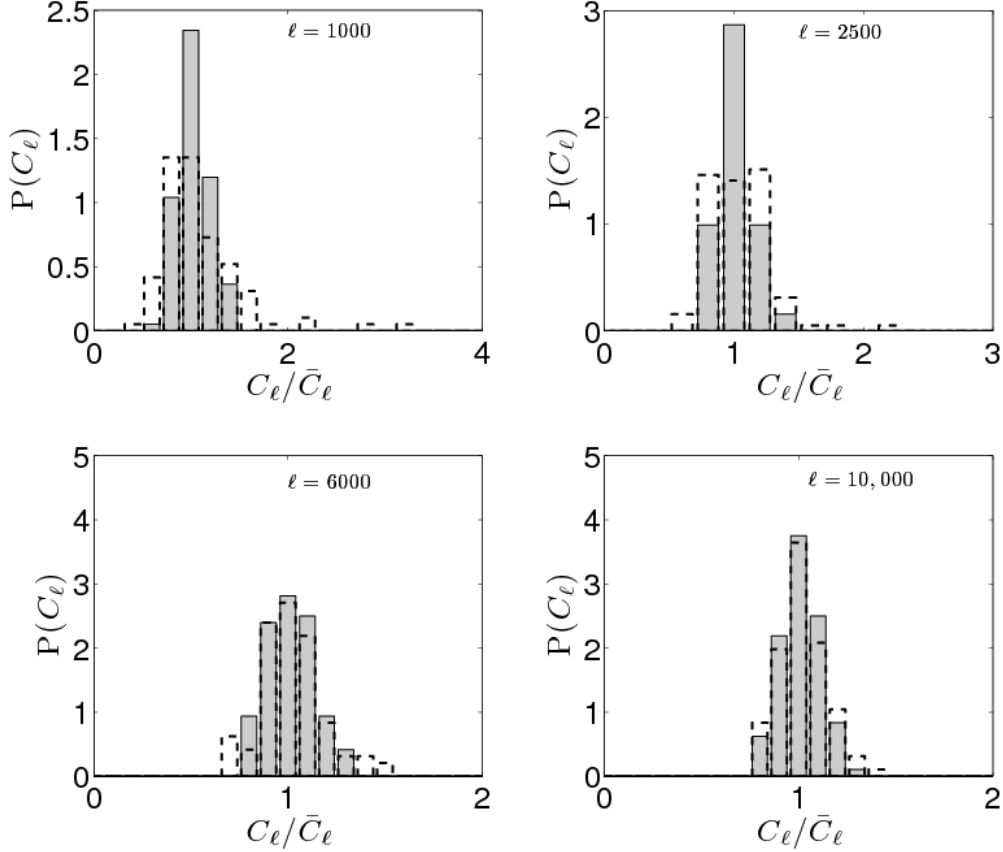


FIG. 7.— The distribution of C_ℓ/\bar{C}_ℓ measured for each simulated BO gas model field in our WMAP3 sample, where \bar{C}_ℓ is the mean over the whole sample of 96 maps, at four different angular multipole numbers: $\ell = 1000, 2500, 6000$ and $10,000$. The unshaded, dashed histogram shows the results without masking clusters. The shaded histogram represents results having masked the brightest 0.9 clusters/deg² from the maps.

on the sky, $C_{\ell,\text{sky}}$, where

$$C_{\ell,\text{sky}} = C_{\ell,\text{SZ}} + C_{\ell,\text{CMB}} + C_{\ell,\text{PS}} + C_{\ell,\text{inst}}, \quad (5)$$

then one can simply remove the foreground components from the measured power spectrum, and clipping the bright clusters will improve the precision on the measured $C_{\ell,\text{SZ}}$. On the other hand, if the error due to cosmic variance on $C_{\ell,\text{CMB}}$ or $C_{\ell,\text{PS}}$ is comparable to $\sigma(C_{\ell,\text{SZ}})$ then reducing the amplitude of the SZ signal by masking clusters may degrade the measured SZ power spectrum amplitude.

For mm-wavelength experiments, the variance on the total power spectrum due to all sources can be written as the sum in quadrature of the Gaussian sample variance term (including CMB, point sources, Gaussian SZ error and instrument noise), the non-Gaussian SZ error and a theory error,

$$\sigma^2(C_{\ell,\text{sky}}) = (\sigma_{\text{cmb}} + \sigma_{\text{sz,G}} + \sigma_{\text{ps}} + \sigma_{\text{inst}})^2 + \sigma_{\text{sz,nG}}^2 + \sigma_{\text{th}}^2, \quad (6)$$

where we have included an error on the predicted SZ power spectrum, σ_{th}^2 , due to the uncertainties in modeling cluster gas physics. Using Eqn. 3 this can be rewritten as

$$\frac{\sigma^2(C_{\ell,\text{sky}})}{(MC_{\ell,\text{SZ}})^2} = \frac{2f_{\text{sky}}^{-1}}{(2\ell + 1)\Delta\ell} [(1 + F/M)^2 + s^2] + t^2, \quad (7)$$

where $s(\ell, n_{\text{th}}) = \sigma_{\text{nG}}/\sigma_{\text{G}}$ and $M(\ell, n_{\text{th}})$ is the ratio of the masked to unmasked $C_{\ell,\text{SZ}}$'s for a given mask surface density threshold n_{th} , and t is the fractional error on $C_{\ell,\text{SZ}}$ due to the theoretical uncertainties in cluster gas physics. F is defined as the ratio of foreground to SZ power,

$$F(\ell) = \frac{C_{\ell,\text{CMB}} + C_{\ell,\text{PS}} + B^{-2}C_{\ell,\text{inst}}}{C_{\ell,\text{SZ}}}, \quad (8)$$

where B is the Fourier domain profile of the telescope beam. We henceforth assume a 10% theoretical uncertainty on C_ℓ , and $10\mu\text{K}$ instrument noise in an arcminute pixel for a single-frequency survey at 90GHz of 25 deg² of sky with a Gaussian beam of FWHM 1.67 arcminutes. The values of s are measured from our WMAP3 simulation SZ map sample, with $\Delta\ell = 300$. The point source power spectrum is calculated assuming radio and sub-mm source populations and spectral index distributions as given in de Zotti et al. (2005) and Negrello et al. (2007).

The upper panel of Figure 8 shows the total fractional error on $\hat{C}_{\ell,\text{SZ}}$ as a function of angular multipole number. The solid black line gives the total fractional error (as given in Eqn. 7) for no masking ($M = 1$). The black dot-dashed, dashed and dotted lines show the contribution of the SZ trispectrum, the total error on the combined

foreground signals (including instrument noise), and the theory uncertainty on C_ℓ , respectively. The red lines show the contributions of the CMB plus Gaussian SZ variance (dashed) and that of the point sources and instrument noise (dotted). It is evident that in the range $2300 < \ell < 5000$ the non-Gaussian variance in the SZ power spectrum amplitude is the dominant source of error on $C_{\ell,SZ}$, with cosmic variance in the CMB power dominating at larger scales, and that of the point sources and instrument noise dominating at smaller scales. It is clear that in this range, $C_{\ell,SZ}$ can be more accurately measured if one can reduce the non-Gaussian variance σ_{nG} by masking clusters.

The lower panel of Figure 8 demonstrates the reduction in the fractional error on $C_{\ell,SZ}$ having masked bright clusters down to the surface density threshold n_{th} (given in the legend), compared to the unmasked case. For $\ell < 2000$, the Gaussian variance on the CMB amplitude dominates and so masking down to 0.1 clusters deg^{-2} (dashed line) merely reduces the amplitude of the SZ signal with no associated reduction in the error ($\sigma(C_\ell)$). Thus the total fractional error increases relative to the unmasked case. However, masking clusters down to 0.25 per square degree (dotted) gives a 20% reduction in the fractional error on $C_{\ell,SZ}$ compared to the unmasked case in the range $3000 < \ell < 4000$. We have found that 0.9 clusters deg^{-2} (dash-dotted) gives the best results; more aggressive masking reduces the amplitude of the SZ power to the point at which the error on the foregrounds becomes significant. Above $\ell = 6000$, the variance due to point sources and instrument noise dominates and so masking clusters simply diminishes the amplitude of the SZ signal without an associated reduction in the variance. As at $\ell < 2000$, this results in a decreased sensitivity to $C_{\ell,SZ}$ at these scales. The red dotted line shows the reduction in the fractional error (for $n_{th} = 0.9$) if one can perfectly remove the primary CMB contribution using multi-frequency observations.

Overall, our results show that, after accounting for the various foregrounds, for a simulated single frequency survey with $10\mu K$ instrumental noise a 20% improvement in the measurement of the amplitude of the SZ angular power spectrum can be obtained if one masks out the brightest clusters from the map down to a surface density threshold of at least 0.25 clusters deg^{-2} . This corresponds to a reduction of $\approx 3\%$ on the error on σ_8 , although we note the additional gain in the Gaussianized statistics of $P(C_{\ell,SZ})$.

5. CONCLUSIONS

We have demonstrated that the SZ power spectrum has a significant amount of variance contributed by rare massive clusters. While these objects do not contribute heavily to the ensemble-average SZ power spectrum, they do add significant non-Gaussian noise to measurements of the power spectrum amplitude and thus degrade cosmological utility. Furthermore, it is difficult to use numerical simulations to characterize the statistics of the SZ power spectrum because one must have sufficiently large volumes to be able to adequately sample the rarest objects in the Universe. We have also shown that the magnitude and scale dependence of the non-Gaussian variance is sensitive to the modelling of the intra-cluster gas.

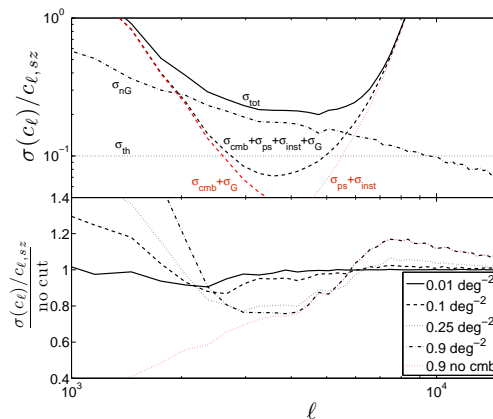


FIG. 8.— (Upper) Fractional error on $C_{\ell,SZ}$ as a function of angular multipole number. The solid black line gives the total fractional error as given in Eqn. 7. The black dot-dashed, dashed and dotted lines show the contributions of the SZ trispectrum, the combined foreground signals (plus Gaussian SZ variance), and the theory uncertainty on C_ℓ , respectively. The red dashed line shows the contribution of just the primary CMB and Gaussian SZ variance; the red dotted line shows that of the point sources plus instrument noise. (Lower) The total fractional error on $C_{\ell,SZ}$ having masked bright clusters from the map divided by the error on $C_{\ell,SZ}$ having applied no masking. In the range $3000 < \ell < 6000$ (where the SZ trispectrum is the dominant error) removing bright clusters from the map increases the precision of measurements of the SZ power spectrum.

A simple solution is to mask out the largest objects in the map before estimating the power spectrum. We have demonstrated using both halo model calculations and a large sample of simulated SZ sky maps that fairly conservative masking can reduce the variance and Gaussianize the statistics significantly, increasing the precision of the measured C_ℓ and thus the sensitivity to cosmological parameters. For example, masking the 10 brightest clusters in a 100 deg^2 SZ map will improve the precision on C_ℓ by a factor of two at $\ell = 1000$ and 1.5 at $\ell = 2000$. Masking the 90 brightest clusters in the same region should improve the accuracy by the same factors at $\ell = 2000$ and 4000 . This is in agreement with work related to information content in the matter power spectrum in the trans-linear regime, where it has been found that a few massive objects are responsible for much of the variance (Neyrinck & Szapudi 2008). Takada & Bridle (2007) have also demonstrated that knowledge of the number of massive clusters within a given survey field can help improve the precision of measurements of the weak lensing shear power spectrum.

Choosing which objects to mask is non-trivial; we found that using a fixed sky density produced a well-defined and well-behaved estimate that can easily be applied to real maps. This skirts the issue (at least partially) of finding an observable that is well-correlated with mass, and can be easily applied to any survey (for example, weak lensing).

We have also shown that the non-Gaussian variance in the SZ power spectrum remains a significant source of error in the range $2300 < \ell < 5000$, even in the presence of the astrophysical foregrounds provided by the primary CMB temperature anisotropies and unresolved point source populations. We have demonstrated that even single frequency experiments with no ability to spectrally subtract the CMB and point sources, can improve

the accuracy on $C_{\ell, sz}$ by more than 20% in the range $3000 < \ell < 4000$ by masking the brightest clusters down to between 0.25 and 0.9 clusters per square degree.

We emphasize that one is not losing cosmological information by masking bright clusters since our procedure is a way to discard the signal from massive clusters whose information we do not know how to analyze but which still contributes to the variance. Halo model calculations of the SZ power spectrum demonstrate that the ensemble-averaged power spectrum ($C_{\ell, sz}$) – to which high mass clusters do not contribute significantly – has a sensitive dependence on σ_8 (Komatsu & Seljak 2002). If one had prior knowledge of the number density and gas properties of clusters over a wide mass and redshift range it would be possible to construct an optimal power spectrum estimator in which the signal from high mass clusters would be down-weighted. However, in this case one would already know the cluster mass function – which is more sensitive to cosmological parameters – and thus power spectrum measurements would reveal no additional information. In the absence of complete knowledge of the mass function, one can simply apply zero weight to the brightest clusters as they effectively contribute only noise to the power spectrum. On the other hand, masked clusters carry much statistical weight when

used to measure the cluster mass function.

There are still theory challenges to predicting the detailed shape and amplitude of the SZ power spectrum, but we have demonstrated that the field-to-field variance can be reduced to allow precise tests of the physics and astrophysics involved.

6. ACKNOWLEDGMENTS

This work supported by the Natural Sciences and Engineering Research Council (Canada) through the Discovery Grant Awards to GPH. GPH would also like to acknowledge support from the Canadian Institute for Advanced Research and the Canada Research Chairs Program. This research was facilitated in part by allocations of time on the COSMOS supercomputer at DAMTP in Cambridge, a UK-CCC facility supported by HEFCE and PPARC. Computer simulations were supported by the National Science Foundation through TeraGrid resources provided by Pittsburgh Supercomputing Center and the National Center for Supercomputing Applications under grant AST070015. We would like to thank Paul Bode for providing the N-body simulations, and Niayesh Afshordi, Keith Vanderlinde, Paul Bode and Nicholas Hall for useful discussions.

REFERENCES

- Arnaud, M., Pointecouteau, E., & Pratt, G. W. 2005, *A&A*, 441, 893
- Ascasibar, Y., Sevilla, R., Yepes, G., Müller, V., & Gottlöber, S. 2006, *MNRAS*, 371, 193
- Barbosa, D., Bartlett, J. G., Blanchard, A., & Oukbir, J. 1996, *A&A*, 314, 13
- Battye, R. A. & Weller, J. 2003, *Phys. Rev. D*, 68, 083506
- Birkinshaw, M. 1999, *Physics Reports*, 310, 97
- Bode, P., Ostriker, J. P., Weller, J., & Shaw, L. 2007, *ApJ*, 663, 139
- Bryan, G. L. & Norman, M. L. 1998, *ApJ*, 495, 80
- Carlstrom, J. E., Holder, G. P., & Reese, E. D. 2002, *ARA&A*, 40, 643
- Cooray, A. 2001, *Phys. Rev. D*, 64, 063514
- da Silva, A. C., Kay, S. T., Liddle, A. R., Thomas, P. A., Pearce, F. R., & Barbosa, D. 2001, *ApJ*, 561, L15
- Dawson, K. S., Holzapfel, W. L., Carlstrom, J. E., Joy, M., & LaRoque, S. J. 2006, *Astrophys. J.*, 647, 13
- de Zotti, G., Ricci, R., Mesa, D., Silva, L., Mazzotta, P., Toffolatti, L., & González-Nuevo, J. 2005, *A&A*, 431, 893
- Dunkley, J., Komatsu, E., Nolta, M. R., Spergel, D. N., Larson, D., Hinshaw, G., Page, L., Bennett, C. L., Gold, B., Jarosik, N., Weiland, J. L., Halpern, M., Hill, R. S., Kogut, A., Limon, M., Meyer, S. S., Tucker, G. S., Wollack, E., & Wright, E. L. 2009, *ApJS*, 180, 306
- Friedman, R. B. & QUaD Collaboration. 2009, in *American Astronomical Society Meeting Abstracts*, Vol. 213, American Astronomical Society Meeting Abstracts, 340.06+
- Gastaldello, F., Buote, D. A., Humphrey, P. J., Zappacosta, L., Bullock, J. S., Brighenti, F., & Mathews, W. G. 2007, *ApJ*, 669, 158
- Herranz, D., Sanz, J. L., Hobson, M. P., Barreiro, R. B., Diego, J. M., Martínez-González, E., & Lasenby, A. N. 2002, *MNRAS*, 336, 1057
- Holder, G. P. & Carlstrom, J. E. 1999, in *Astronomical Society of the Pacific Conference Series*, Vol. 181, *Microwave Foregrounds*, ed. A. de Oliveira-Costa & M. Tegmark, 199+
- Holder, G. P. & Carlstrom, J. E. 2001, *ApJ*, 558, 515
- Holder, G. P., Mohr, J. J., Carlstrom, J. E., Evrard, A. E., & Leitch, E. M. 2000, *ApJ*, 544, 629
- Jenkins, A., Frenk, C. S., White, S. D. M., Colberg, J. M., Cole, S., Evrard, A. E., Couchman, H. M. P., & Yoshida, N. 2001, *MNRAS*, 321, 372
- Komatsu, E. & Seljak, U. 2002, *MNRAS*, 336, 1256
- Kosowsky, A. 2003, *New Astronomy Review*, 47, 939
- Lima, M. & Hu, W. 2005, *Phys. Rev. D*, 72, 043006
- Lin, Y.-T., Mohr, J. J., & Stanford, S. A. 2003, *ApJ*, 591, 749
- Majumdar, S. & Mohr, J. J. 2003, *ApJ*, 585, 603
- Melin, J.-B., Bartlett, J. G., & Delabrouille, J. 2006, *A&A*, 459, 341
- Motl, P. M., Hallman, E. J., Burns, J. O., & Norman, M. L. 2005, *ApJ*, 623, L63
- Nagai, D. 2006, *ApJ*, 650, 538
- Nagamine, K., Ostriker, J. P., Fukugita, M., & Cen, R. 2006, *ApJ*, 653, 881
- Negrello, M., Perrotta, F., González-Nuevo, J., Silva, L., de Zotti, G., Granato, G. L., Baccigalupi, C., & Danese, L. 2007, *MNRAS*, 377, 1557
- Neyrinck, M. C. & Szapudi, I. 2008, *MNRAS*, 384, 1221
- Nozawa, S., Itoh, N., Suda, Y., & Ohhata, Y. 2006, *Nuovo Cimento B Serie*, 121, 487
- O'Hara, T. B., Mohr, J. J., Bialek, J. J., & Evrard, A. E. 2006, *ApJ*, 639, 64
- Ostriker, J. P., Bode, P., & Babul, A. 2005, *ApJ*, 634, 964
- Ruhl, J., Ade, P. A. R., Carlstrom, J. E., Cho, H.-M., Crawford, T., Dobbs, M., Greer, C. H., Halverson, N. w., Holzapfel, W. L., Lanting, T. M., Lee, A. T., Leitch, E. M., Leong, J., Lu, W., Lueker, M., Mehl, J., Meyer, S. S., Mohr, J. J., Padin, S., Plagge, T., Pryke, C., Runyan, M. C., Schwan, D., Sharp, M. K., Spieler, H., Staniszewski, Z., & Stark, A. A. 2004, in *Society of Photo-Optical Instrumentation Engineers (SPIE) Conference Series*, Vol. 5498, *Society of Photo-Optical Instrumentation Engineers (SPIE) Conference Series*, ed. C. M. Bradford, P. A. R. Ade, J. E. Aguirre, J. J. Bock, M. Dragovan, L. Duband, L. Earle, J. Glenn, H. Matsuvara, B. J. Naylor, H. T. Nguyen, M. Yun, & J. Zmuidzinas, 11–29
- Schäfer, B. M. & Bartelmann, M. 2007, *MNRAS*, 377, 253
- Schäfer, B. M., Pfrommer, C., Hell, R. M., & Bartelmann, M. 2006, *MNRAS*, 370, 1713
- Sehgal, N., Trac, H., Huffenberger, K., & Bode, P. 2007, *ApJ*, 664, 149
- Sharp, M. K., Marrone, D. P., Carlstrom, J. E., Culverhouse, T., Greer, C., Hawkins, D., Hennessy, R., Joy, M., Lamb, J. W., Leitch, E. M., Loh, M., Miller, A., Mroczkowski, T., Muchovej, S., Pryke, C., & Woody, D. 2009, *ArXiv e-prints*
- Shaw, L. D., Holder, G. P., & Bode, P. 2008, *ApJ*, 686, 206

- Sievers, J. L., Mason, B. S., Weintraub, L., Achermann, C., Altamirano, P., Bond, J. R., Bronfman, L., Bustos, R., Contaldi, C., Dickinson, C., Jones, M. E., May, J., Myers, S. T., Oyarce, N., Padin, S., Pearson, T. J., Pospieszalski, M., Readhead, A. C. S., Reeves, R., Shepherd, M. C., Taylor, A. C., & Torres, S. 2009, ArXiv e-prints
- Spergel, D. N., Bean, R., Doré, O., Nolta, M. R., Bennett, C. L., Dunkley, J., Hinshaw, G., Jarosik, N., Komatsu, E., Page, L., Peiris, H. V., Verde, L., Halpern, M., Hill, R. S., Kogut, A., Limon, M., Meyer, S. S., Odegard, N., Tucker, G. S., Weiland, J. L., Wollack, E., & Wright, E. L. 2007, ApJS, 170, 377
- Staniszewski, Z., Ade, P. A. R., Aird, K. A., Benson, B. A., Bleem, L. E., Carlstrom, J. E., Chang, C. L., Cho, H. ., Crawford, T. M., Crites, A. T., de Haan, T., Dobbs, M. A., Halverson, N. W., Holder, G. P., Holzzapfel, W. L., Hrubes, J. D., Joy, M., Keisler, R., Lanting, T. M., Lee, A. T., Leitch, E. M., Loehr, A., Lueker, M., McMahon, J. J., Mehl, J., Meyer, S. S., Mohr, J. J., Montroy, T. E., Ngeow, C. ., Padin, S., Plagge, T., Pryke, C., Reichardt, C. L., Ruhl, J. E., Schaffer, K. K., Shaw, L., Shirokoff, E., Spieler, H. G., Stalder, B., Stark, A. A., Vanderlinde, K., Vieira, J. D., Zahn, O., & Zenteno, A. 2008, ArXiv e-prints
- Takada, M. & Bridle, S. 2007, New Journal of Physics, 9, 446
- Vikhlinin, A., Kravtsov, A., Forman, W., Jones, C., Markevitch, M., Murray, S. S., & Van Speybroeck, L. 2006, ApJ, 640, 691
- Vikhlinin, A., Kravtsov, A. V., Burenin, R. A., Ebeling, H., Forman, W. R., Hornstrup, A., Jones, C., Murray, S. S., Nagai, D., Quintana, H., & Voevodkin, A. 2009, ApJ, 692, 1060
- Voevodkin, A. & Vikhlinin, A. 2004, ApJ, 601, 610
- White, M., Hernquist, L., & Springel, V. 2002, ApJ, 579, 16
- Zhang, P. & Sheth, R. K. 2007, ApJ, 671, 14
- Zhang, Y.-Y., Finoguenov, A., Böhringer, H., Kneib, J.-P., Smith, G. P., Czoske, O., & Soucail, G. 2007, A&A, 467, 437